

RESEARCH ARTICLE

# Automatic diagnostics of tuberculosis using convolutional neural networks analysis of MODS digital images

Santiago Lopez-Garnier<sup>1,2</sup>, Patricia Sheen<sup>1</sup>, Mirko Zimic<sup>1\*</sup>

**1** Unidad de Bioinformática / Laboratorio de Enfermedades Infecciosas, Laboratorio de Investigación y Desarrollo, Facultad de Ciencias y Filosofía—Universidad Peruana Cayetano Heredia, Lima, Peru, **2** Wyss Institute for Biologically Inspired Engineering, Harvard University, Cambridge, Massachusetts, United States of America

\* [mirko.zimic@upch.pe](mailto:mirko.zimic@upch.pe)



**OPEN ACCESS**

**Citation:** Lopez-Garnier S, Sheen P, Zimic M (2019) Automatic diagnostics of tuberculosis using convolutional neural networks analysis of MODS digital images. PLoS ONE 14(2): e0212094. <https://doi.org/10.1371/journal.pone.0212094>

**Editor:** Ivan Olier, Liverpool John Moores University, UNITED KINGDOM

**Received:** November 10, 2017

**Accepted:** January 26, 2019

**Published:** February 27, 2019

**Copyright:** © 2019 Lopez-Garnier et al. This is an open access article distributed under the terms of the [Creative Commons Attribution License](https://creativecommons.org/licenses/by/4.0/), which permits unrestricted use, distribution, and reproduction in any medium, provided the original author and source are credited.

**Data Availability Statement:** All of the datasets, optimized models, parameters, generated images, extracted features and scripts are available for download (Google Drive links) via our Github page: [https://github.com/santiagolopezg/MODS\\_ConvNet/tree/master/STM\\_Code](https://github.com/santiagolopezg/MODS_ConvNet/tree/master/STM_Code). The code is available, and to download the aforementioned files, users are to read the Download files document: [https://github.com/santiagolopezg/MODS\\_ConvNet/blob/master/STM\\_Code/download\\_files.md](https://github.com/santiagolopezg/MODS_ConvNet/blob/master/STM_Code/download_files.md). In addition to this, the authors have included urls in the manuscript that allow for direct access to all datasets, models, and code.

## Abstract

Tuberculosis is an infectious disease that causes ill health and death in millions of people each year worldwide. Timely diagnosis and treatment is key to full patient recovery. The Microscopic Observed Drug Susceptibility (MODS) is a test to diagnose TB infection and drug susceptibility directly from a sputum sample in 7–10 days with a low cost and high sensitivity and specificity, based on the visual recognition of specific growth cording patterns of *M. Tuberculosis* in a broth culture. Despite its advantages, MODS is still limited in remote, low resource settings, because it requires permanent and trained technical staff for the image-based diagnostics. Hence, it is important to develop alternative solutions, based on reliable automated analysis and interpretation of MODS cultures. In this study, we trained and evaluated a convolutional neural network (CNN) for automatic interpretation of MODS cultures digital images. The CNN was trained on a dataset of 12,510 MODS positive and negative images obtained from three different laboratories, where it achieved 96.63 +/- 0.35% accuracy, and a sensitivity and specificity ranging from 91% to 99%, when validated across held-out laboratory datasets. The model's learned features resemble visual cues used by expert diagnosticians to interpret MODS cultures, suggesting that our model may have the ability to generalize and scale. It performed robustly when validated across held-out laboratory datasets and can be improved upon with data from new laboratories. This CNN can assist laboratory personnel, in low resource settings, and is a step towards facilitating automated diagnostics access to critical areas in developing countries.

## Introduction

Tuberculosis (TB) is a global and lethal disease, responsible for the ill-health and death of more than 1.4 million deaths each year, ranking above HIV/AIDS as one of the leading causes of death from an infectious disease [1,2]. Timely diagnosis and treatment is key to full patient recovery. About a third of the global population is affected by latent TB infection, and it is believed that around 5–10% of the people develop active TB during their life [3]. Recently,

They would like to state that funding from Google does not alter their adherence to PLOS ONE policies on sharing data and materials.

**Funding:** This study was funded by The Wellcome Trust 099805/Z/12/Z, <https://wellcome.ac.uk> (PS) and by the Google Latin American Research Award 2016 <https://research.google.com> (MZ). PS was funded by a Wellcome Trust Intermediate Fellowship. The funders had no role in study design, data collection and analysis, decision to publish, or preparation of the manuscript.

**Competing interests:** The funding received from Google: we would like to declare that this does not alter our adherence to PLOS ONE policies on sharing data and materials.

there has been a surge of multi drug resistant TB (MDR-TB), due to lack of early diagnostics, ineffective susceptibility tests and inappropriate treatments [4]. Worse still, we are now facing extreme-drug resistant strains (XDR-TB), which are bacillus with acquired resistance to the most potent anti tuberculous drugs [5,6]. Timely diagnosis, recognition of MDR, and treatment initiation are key to improve patient recovery.

In 2011, the WHO began to back a diagnostics test for TB, called MODS (Microscopic Observed Drug Susceptibility) [5,7]. This low-cost method is based on the identification of *M. tuberculosis* (MTB) growth in broth in 7–10 days from a sputum sample. A characteristic S shaped, cord-like morphology of colonies in the culture evidences the presence of TB (Fig 1). A typical TB cord in a positive MODS culture exhibits certain morphological and illumination characteristics. A TB positive cord has a particular length and width, and its shape is usually sinuous with a smooth border. Given that a TB cord has a circular transversal section, the light that passes through the diameter shows a high-transmitted brightness, while the light that passes through the border, gets refracted resulting in a lower brightness (Fig 1).

Notably, besides TB detection, MODS is able to simultaneously detect MDR-TB, and XDR-TB with high sensitivity and specificity [7]. Despite its advantages, MODS has a main limitation: the interpretation must be performed by trained personnel, who are often unavailable in low resource settings, which coincidentally are the areas most prone to tuberculosis infections.

In our previous study, a feature-based logistic regression pattern recognition algorithm to automatically interpret MODS digital images was developed [8]. The algorithm used extensive image processing, feature extraction and pattern recognition. It searched for geometrical and illumination features that correspond to those considered by human experts for classification, and was able to detect TB with 99.1% sensitivity and 99.7% specificity [8]. Despite the model's in-sample accuracy, its performance significantly dropped to 92% when tested on digital images from a held out laboratory. This limitation is caused by the variability in the image's background quality, when samples are processed in different laboratories. Hence, the model required retraining to be deployable at a new laboratory (Zimic M, to be published).

In recent years, advances in machine learning and the implementation of convolutional neural networks (CNNs), paired with the assembly of increasingly complex datasets, have enhanced object classification and detection capabilities [9,10]. CNNs are biologically-inspired hierarchical models capable of making strong assumptions about locality of pixel dependencies in images [11], by learning spatially informed feature hierarchies [10,12]. They consist of feature detector units arranged in layers: lower layers detect simple features and feed into higher layers, which detect more complex features [10,12]. There is compelling evidence that such models can match or outperform human experts on complex tasks, such as image and text

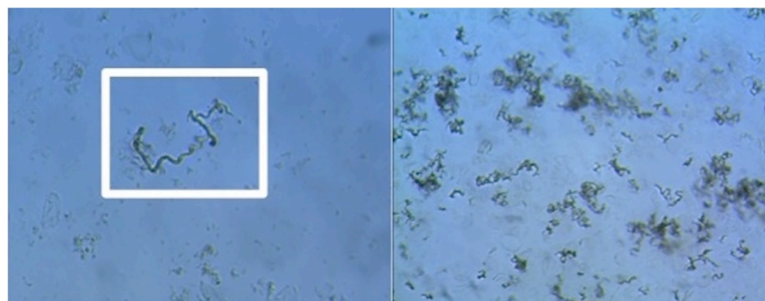


**Fig 1. Examples of positive images.** On the left, a characteristic *M. tuberculosis* chord is highlighted in the white box. On the right, a typical image of a positive MODS culture. Notice the chord shaped growth morphology.

<https://doi.org/10.1371/journal.pone.0212094.g001>

processing, recognition and classification [9,10,13–15], decision-making based on abstract representations [16,17], and even decision-making in clinical settings [18,19]. Due to the recent availability of increasingly large medical datasets, it has become possible to develop CNN models for Computer-Aided Diagnosis, and uses in routine clinical applications. These include temporal convolutional networks for disease pattern discovery [20]; detection of glaucoma [21]; detection and analysis of potential breast cancer masses [22,23]; and the classification of skin lesions for the detection of skin cancer [18], amongst others.

Tuberculosis control efforts are hampered by a mismatch in diagnostic technology: modern optimal diagnostic tests are least available in poor areas where they are needed most. Lack of adequate early diagnostics and MDR detection is a critical problem in control efforts.

As explained above, despite MODS being an important test for the diagnostics of TB and MDR, an important limitation that laboratories in the developing world face in MODS implementation is the presence of permanent technical staff with expertise in reading MODS. Based on a dataset of more than 12000 images, we designed and trained a CNN for automatic identification of MTB colonies in a MODS culture. Our computational tool can assist laboratory personnel in MODS interpretation, or substitute for the absence of diagnosticians in low resource settings through teleradiology.

## Materials and methods

### Dataset composition and structure

**Primary dataset.** Our primary dataset is composed of MODS digital images obtained from the images bank of the Bioinformatics and Molecular Biology Laboratory at UPCH. The MODS cultures and their posterior digitalization were performed in 3 laboratories from the cities of Trujillo, Callao and Lima (UPCH), in Peru, during a previous study (to be published). In that study, each image was assigned a label, positive or negative, by three experts independently. Images in which MTB growth was detected by at least 2 experts were considered positive, and were considered negative if the 3 experts classified them correspondingly. The images were 2048×1536 pixel RGB. To build the dataset, Trujillo provided 9,005 images; Callao provided 5,670 images; and UPCH provided 608 images. After eliminating unreadable images, we ended up with a dataset of 12,510 images: 4,849 positive and 7,661 negative images. Images were rescaled to 224 x 224 pixels, and converted to grayscale. We avoided further image pre-processing, due to the fear of introducing visual artifacts into images of already heterogeneous quality and background (see Fig 1). Additionally, this would allow us to evaluate our CNN's ability to operate on raw data.

In order to prevent any overlap or bias between training and validation sets of data, and to allow a robust assessment of the model's performance with reliable metrics, we performed 5-fold cross-validation. This was achieved by segmenting the original 12,510 image dataset into 5 subsets, composed of 2,502 images each. These subsets were selected randomly from the original dataset, following a 0.63 positive:negative ratio. For each cross-validation step, we used 4 subsets for training/validation (10,008 images), and 1 subset for testing (2,502 images). This allowed the network to train with different images during each round of cross-validation, and to evaluate its performance on unseen images. Models trained on this dataset are referred to as "resc\_CNN". Images corresponding to TB-positive and TB-negative categories, may show different levels of complexity, turning them into images with strong or weak evidence for classification. Fig 2 illustrates the difficulty in correctly classifying images, both in the TB-positive and TB-negative categories.

**Secondary dataset (paired-laboratory dataset).** In order to demonstrate the model's robustness and ability to generalize, we trained it on two laboratories worth of images, and had

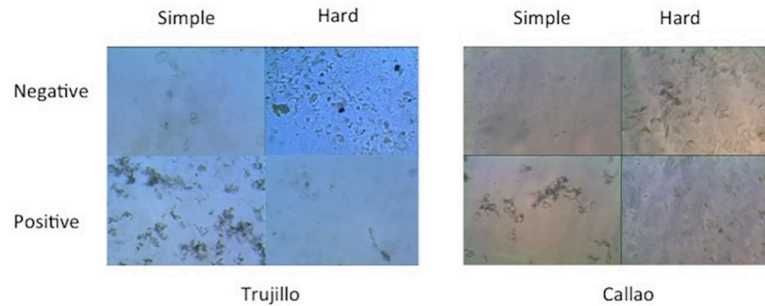


**Fig 2. Examples from 2 of the 3 datasets (Trujillo and Callao) of positive and negative frames.** We've selected a few images from each dataset to illustrate the difficulty in correctly classifying each image. First column images are from Trujillo; the second column images are from Callao. Notice how similar contaminated negative samples are to relatively clean positive samples.

<https://doi.org/10.1371/journal.pone.0212094.g002>

it predict the label of images from a third, held out laboratory's images. Hence, we generated secondary cross-validation datasets, where we grouped laboratory images in pairs, as follows: group 1 was composed of 8092 images from Callao and Trujillo for the network training, and 484 images from UPCH for validation; group 2, 3400 images from Callao and UPCH for training, and 6004 from Trujillo for validation; group 3, 5518 images from Trujillo and UPCH for training, and 3512 from Callao for validation. These large datasets were then segmented into 5 folds, and 5 cross-validation datasets were generated as described above. Models trained on this dataset are referred to as "2lab\_CNN". Both of these datasets are available for download [here](#).

### Network architecture

Our network was designed as a 15-layer deep convolutional neural network, comprising convolutional, max-pooling and fully-connected layers. The CNN architecture is organised in 5 blocks: 4 convolutional and 1 fully-connected/classification blocks, separated by pooling layers (Fig 3). The network was written in Python using Keras high-level neural networks library [24], and used Theano [25] as a backend. The code is available [here](#).

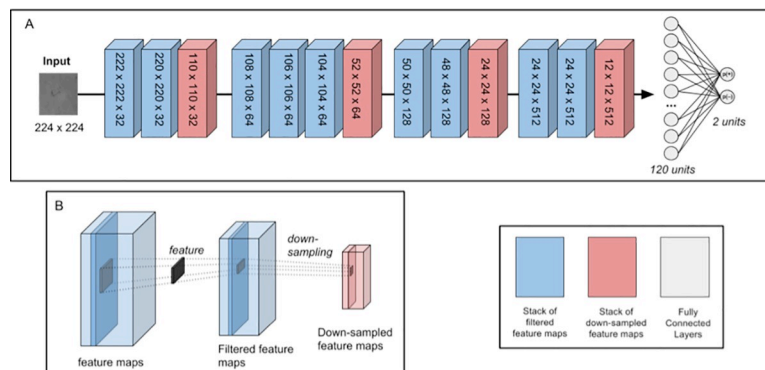


**Fig 3. Simplified network architecture.** (A) Input to the network is a 224 x 224 grayscale image of a MODS *M. tuberculosis* culture. The image is passed through the network, and the output of the second fully-connected layer is a probability distribution over the two classes (positive (+): 1 and negative (-): 0). Each block is a stack of feature maps, of dimensions (width x height x number of feature maps). Layer operations take place between each block (see (B)) and are identifiable by the feature map volume produced. Kernels are 3 x 3 and 2 x 2 for convolutional and pooling layers, respectively. The network is trained and evaluated on a dataset of 1008 train/validation and 2502 test images. (B) A schematic representation of the convolution and pooling operations on an input volume. Note that each convolution operation shown in the figure represents the Conv-BatchNorm-Activation operations.

<https://doi.org/10.1371/journal.pone.0212094.g003>

The architecture itself is an adaptation of the VGG16 network, proposed by Simonyan [26], which pioneered the use of deep, multi-layered CNNs with small convolutional filter kernels. This approach has been previously favored, notably by Szegedy's entry of the ILSVRC-2014 classification task, GoogleNet [9]. It allows the incorporation of multiple non-linear rectification (ReLU) layers in the place of a single one, making the decision function more discriminative. Additionally, it allows for a decrease in the number of parameters to be fine-tuned. We hypothesized that, due to the inherent complexity of our dataset and the need for precise feature extraction, these models were promising templates for experimentation. The architecture was fine-tuned by hyperparameter search and optimization over the basic architecture, and selection of the network that demonstrated best testing accuracy—these iterations can be further explored [here](#).

Input to the network is 1 x 224 x 224, as the images are grayscale. The image dimension was selected because (1) it was the one used by our base model [26], and (2) this was the input that allowed us most flexibility for trying out different variations of filter dimensions and kernel sizes. The conversion to grayscale serves two purposes—firstly, on a practical level, it is less costly in parameters (1 channel vs. 3). Secondly, and perhaps more importantly, we had previously found that certain physical parameters, unrelated to color, were principal predictors of image classification as positive or negative, in a logistic regression model [8]—hence, we reasoned that, if the model were to act as an expert diagnostician and identify similar features (cording characteristics, illumination, edge to surrounding contrast), the variation in color between laboratory datasets would be only be an additional confounding factor, and that we account for it. In other words, we considered that the information we would lose by reducing channels would probably be a source of noise, rather than an important feature for classification.

All of the convolutional layers apply 3 x 3 kernels with stride = 1 to the input volume, mapping features to activation map stacks in deeper layers of the network. This kernel dimension was selected because it allowed to stack more convolution operations per block [27], to obtain a larger, locally dependent receptive field which provide more expressive features [28]. The receptive field of 3 x 3 is the smallest to still capture notions of directionality [26]. This small receptive field convolves the input at each convolutional layer, and allows stacking of convolutional operations. These smaller sized filters have also been used previously by Ciresan et al. [13]. In practice, stacking two 3 x 3 convolutional layers results in an effective receptive field of 5 x 5 [26]. This is interesting, because using two 3 x 3 convolutional layers instead of one 5 x 5 layer allows (1) the incorporation of 2 ReLU activation layers, that make the decision function more discriminative and (2) a decrease in the number of parameters [26]

As the inputs to the convolutional layers do not have spatial padding, there is an effective reduction of 2 pixels in width and height per convolution operation, helping to reduce activation map volumes and therefore the number of parameters optimized. This, paired with spatial pooling (see below) was partly to compensate for the increase in number of tunable parameters due to network depth, the convolutional layers, The kernels' outputs are activation map volumes of dimension (filtered image width x filtered image height x number of filters generated). Because in deeper layers, features become more complex, we doubled the number of filters optimized by each convolutional layer, between each block of layers. As these features become more complex, they map onto larger regions of the input volume, making their role in identifying features in the input data fundamental.

To further allow for feature extraction, we configured the CNN's 4<sup>th</sup> block, comprised by two convolutional layers, to output the same dimensions as their inputs. This maintained the activation map volume at 512 x 24 x 24. This allowed for the filtering over a conserved input volume. Hence, it permits the extraction of more meaningful features from the input [11].



Batch normalisation was used prior to ReLU activation. In our CNN, batch normalisation allowed us to use higher learning rates for network optimisation without the risk of divergence, regardless of weight initialisations; it also accelerates the training of deep neural networks [29]. ReLU nonlinearity also allow for faster training of CNNs, which helps to avoid large models overfitting on smaller datasets [11,27].

Spatial pooling is carried out by 4 max-pooling layers, one at the end of each layer block. Max-pooling operations were performed using 2 x 2 kernels with a stride = 2, as recommended previously [13,26]. This kernel dimension allowed the network to reduce the spatial size of the representation by eliminating non-maximal values, which in turn reduced the number of parameters and computational time; additionally, it helped to control overfitting by providing a form of translation invariance [13,26].

Finally, the fourth convolutional block is followed by two fully-connected layers. The first has 120 units. The second, sigmoid layer, is composed of two units (one per category), that outputs a probability distribution over the two categories (positive (+): 1 and negative (-): 0).

## Training

During the training phase, we provide the model with images belonging to each cross-validation training dataset. Prior to training, we split the training data into training and validation data. The validation data allowed us to monitor our model's performance and select the best model for later testing and performance evaluation. The split was performed to keep 85% of the data for training, and reserve 15% for validation. To increase the number of training samples, we used Keras' data augmentation feature. This generated batches of image data with real-time data augmentation, useful to avoid over-fitting and enhance evaluation of the network's performance, while keeping the original label (positive or negative) of each image [11,13]. The modifications performed on the original images consisted of rotations, width and height shifts (1/10 of the original image), as well as horizontal and vertical flipping of the images. We used He Normal weight initialization, which facilitates convergence, even in very deep convolutional networks [14]. We used Keras' checkpoint feature to create checkpoints of the model's parameters after the training epoch during which our model's validation accuracy was highest. After each training session, a new model instance was called, which reset the previously optimized parameters, and the newly instantiated model was trained on the next dataset. This allowed for objective assessment of the model's reported metrics. In this sense, it is important to note that our models were not trained across all cross-validation datasets: each model trained on a certain fold of the cross-validation datasets (for example, training data from dataset 1) was fine-tuned and tested only with its corresponding test data (test data from dataset 1).

The metric monitored to guide the network towards minimal error loss and create checkpoints was binary cross-entropy loss, calculated by the binary cross-entropy cost function (logloss). For hyperparameter selection, we first performed a hyperparameter search, exhaustively trying combinations of hyperparameters (learning rate, optimizer, batch size and dropout). From this hyperparameter search, we selected the model that demonstrated highest validation metrics. Hence, we ended up using RMSProp with a learning rate =  $10^{-3}$  as the optimizer to minimize the cross entropy loss. The network was trained for 100 epochs, using a batch size of 72, and dropout of 0.5. Dropout prevents units from co-adapting and forces them to learn more robust features by setting to zero the output of a given hidden unit, with a probability of 0.5 [11,30]. The training was conducted on a NVIDIA GeForce GTX TITAN X (12 Gb DDR5 RAM, 512 bits, 3072 cores) GPU. The training lasted 3.5 days for the resc\_CNN, at 700 s per epoch. After the initial training, the network was fine-tuned for 100 more epochs, with RMSprop and a learning rate =  $3 \times 10^{-4}$ .

To evaluate the model's robustness, we performed two rounds of training: first, we trained the `resc_CNN` network with the parameters as described above, on the secondary datasets. After a first round of 100 epochs on 5 sub-datasets per pair of laboratories, we obtained five sets of weights per pair of laboratories. We validated the network on the held out laboratory's images, and selected the set of weights per laboratory pair that allowed for highest validation sensitivity. The second round of training consisted in using these weights to generate new instances of the model, per cross-validation split and per pair of laboratories, and trained the networks for 100 more epochs.

## Network performance validation and metrics

To evaluate the classification performance of our network, we used 5 metrics: the binary accuracy, sensitivity, specificity, Matthews Correlation Coefficient (MCC) and F1 score. The binary accuracy calculates the mean accuracy rate across all predictions for binary classification problems. The sensitivity (or recall) is the fraction of truly positive images that the algorithms classifies positive. The specificity (or true negative rate) is the fraction of truly negative images that the algorithm classifies as negative. The Matthews Correlation Coefficient is a metric used to evaluate the quality of binary classifications. Lastly, the F1 score is a metric that combines precision and recall, relative to the positive (TB) class.

As mentioned previously, we opted to separate training and testing steps, to allow for simultaneous model training and testing. To evaluate our network's performance, we loaded the best model saved by the checkpoint during training, and validated it on unseen images. This validation set varies amongst datasets, and allowed us to perform five cross-validation for the `resc_CNN` models. The mean and standard deviation for each metric were then calculated.

To demonstrate the model's robustness, we loaded the best model saved by the checkpoint feature during the secondary training step on the paired-laboratory dataset of images. Here, each model instance corresponds to the best model generated by a certain fold of cross-validation training on images from a pair of laboratories. The validation images were from the held out laboratory, hence resulting in three `2lab_CNN` models, one per paired-laboratory datasets. The mean and standard deviation for each of the aforementioned metrics on each paired-laboratory datasets were then calculated.

In addition to evaluating the model's performance, we were interested in visualising the features that the model's convolutional layers were optimising. This provides insight into the function of intermediate feature layers, and the evolution of features during training [28]. We achieved this using the filter visualisation script, adapted from Keras' visualization utility. This method relies on maximizing the activation of filters in specific convolutional layers of our model's architecture, after training [31]. Starting with a grayscale image ( $x$ ), the activation ( $a(x)$ ) caused by the input is computed by a loss function, and 100 steps are taken in the input space along the gradient (gradient ascent) to modify the input to cause higher activations [32].

The filters are sorted by descending activations, and the best 49 filters are saved.

Additionally to visualizing features, we synthetically generated input images that would maximize the activation for a specific class—in particular, we were interested in evaluating how the features deemed most useful in label attribution by the model relate to these synthetically generated positive images. To achieve this, we generated negative and positive images that maximized the activations of the 0<sup>th</sup> and 1<sup>st</sup> neurons respectively, in our output classification layer. This is done similarly to the filter visualization procedure: gradient ascent was performed for 2000 steps on noisy gray images, and the top 9 images, sorted by activation, were saved. Here, the activation is the probability assigned by the model's output layer to a generated input that it belongs to the corresponding index (0 or 1) [31].

**Table 1. Cross-validation results for the resc\_CNN model.**

model	cross-validation folds	Binary Accuracy	Sensitivity (Recall)	Specificity	MCC	F1 score
resc_CNN	5	96.63 +/- 0.35%	94.74 +/- 0.89%	97.83 +/- 1.07%	0.8986 +/- 0.0045	0.9562 +/- 0.0041

<https://doi.org/10.1371/journal.pone.0212094.t001>

We were also interested in assessing the possible similarities between features learned by our 3 models generated by the 2-laboratory training / 1 laboratory validation datasets. This was also performed as described above, and we also generated images of positive class for comparison. The generated images, filters, and model parameters are available for download [here](#).

## Results and discussion

### Network performance

Resc\_CNN was trained and tested independently on 5 datasets generated by cross-validation, each composed of 12510 images (10008:2502 training/validation split—data). In each fold, a different fifth of the total dataset is used for testing. The mean and standard deviation from the validation metrics across all 5 of cross-validation were computed over the corresponding testing dataset (Table 1). Our CNN achieved 96.63 +/- 0.35% (mean s.d.) binary accuracy, 94.74 +/- 0.89% sensitivity and 97.83 +/- 1.07% specificity.

Despite the reduced training dataset size, and the difference in quality between images in the training and validation datasets, our three models were able to identify tuberculosis on a held out dataset, with an average 95.76% accuracy, 94.27% sensitivity and 96.81% specificity (Table 2).

Furthermore, in order to identify the features learned by the CNN, we proceeded to visualisation of the features that the model’s convolutional layers were optimizing (Fig 4A).

In addition to extracting features from the resc\_CNN, trained and validated on data from three laboratories, we proceeded to compare features from the last convolutional layer of the three 2lab\_CNN models (Fig 5). Notably, The features extracted from the three models trained on different pairs of data are similar, and resemble the features extracted from the resc\_CNN model.

However, these results are insufficient to claim that the CNN actively uses the features to classify the test images, or that these features are deemed sufficient by the CNN to assign class labels. Therefore, we proceeded to generate synthetic images by gradient ascent, which maximize the activation out of the j<sup>th</sup> layer of the CNN. This image generation can be performed both for the positive and negative classes. For means of comparison, we have also provided real images corresponding to each class for comparison (Fig 4B and Fig 5). The features identified as most useful for classification are visible in the generated positive image.

This study shows that a CNN can be trained ad-hoc to interpret MODS cultures digital images for diagnostics of TB. This network can correctly classify MODS images with high accuracy, sensitivity and specificity.

When evaluating our model’s ability to generalise, we found that when laboratory pair datasets were validated with a third, held out laboratory dataset, the model’s metrics were similar

**Table 2. Cross-validation results for the 2lab\_CNN model.**

model	cross-validation folds	Binary Accuracy	Sensitivity (Recall)	Specificity	MCC	F1 score
2lab_CNN_1	5	99.01 +/- 0.62%	98.60 +/- 1.31%	99.38 +/- 0.77%	0.9681 +/- 0.0223	0.9894 +/- 0.0066
2lab_CNN_2	5	93.24 +/- 1.98%	91.12 +/- 2.34%	94.36 +/- 3.00%	0.8152 +/- 0.0418	0.9022 +/- 0.0265
2lab_CNN_3	5	95.03 +/- 1.14%	93.08 +/- 2.45%	96.69 +/- 1.22%	0.8486 +/- 0.0383	0.9448 +/- 0.0131

<https://doi.org/10.1371/journal.pone.0212094.t002>



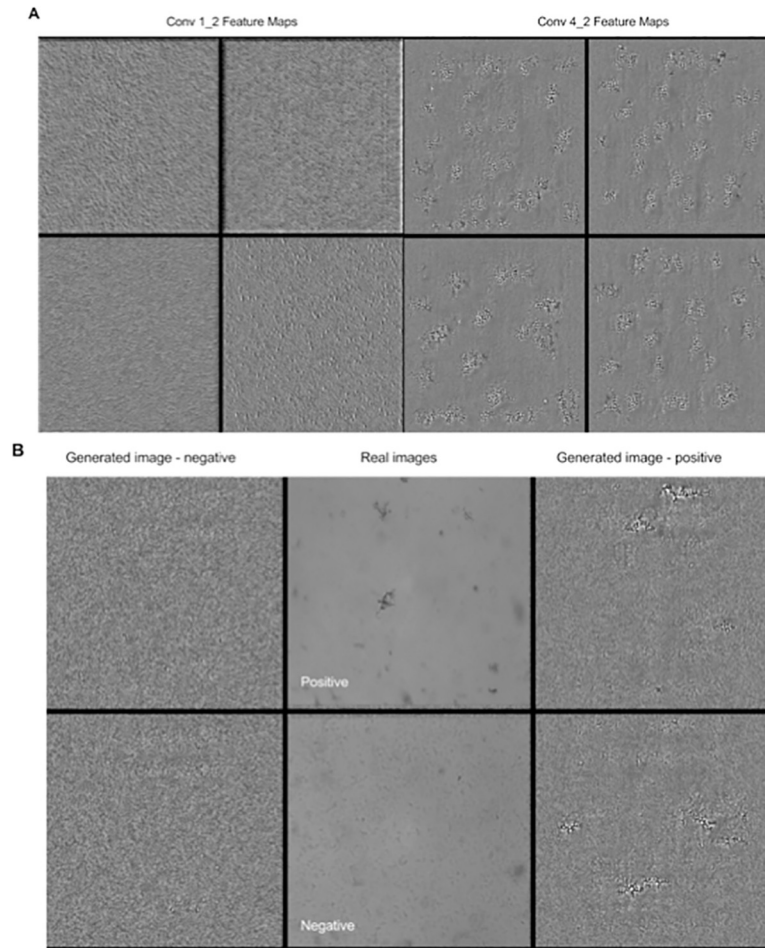


**Fig 4. Features learnt and images synthetically generated by resc\_CNN.** (A) Visualisation of features and comparison of the learnt by convolutional layers. We randomly selected the features that caused top 4 activations across all feature maps of the 2<sup>nd</sup> and 9<sup>th</sup> convolutional layers. (B) Synthetically generated images. Images generated by gradient ascent maximize the activation out of the  $j^{\text{th}}$  layer of the CNN, for the positive and negative classes, alongside examples of positive and negative testing images, as provided to the CNN for classification. The figure is best viewed in digital format, and the full collection of generated features and synthetic images are available [here](https://doi.org/10.1371/journal.pone.0212094.g004).

<https://doi.org/10.1371/journal.pone.0212094.g004>

to what it achieved after training on the whole, shuffled dataset. The UPCH laboratory has the most experience in digitalizing MODS cultures, so images provided by this laboratory are of the highest quality. Intermediate experience and image quality correspond to the Callao laboratory, followed by the Trujillo laboratory, which had just begun to perform MODS cultures during the execution of this study. The three models tested achieved  $\geq 90\%$  sensitivity and specificity, despite the reduced training dataset size, and the difference in quality between images in the training and validation datasets (Table 2).

Furthermore, we found that the model's learned features resemble visual cues used by expert diagnosticians to identify MODS cording patterns. Within these features, the cording shapes and edges are identifiable, and these resemble *M. tuberculosis*' characteristic growth in MODS culture (Fig 4A). The first convolutional layer appears to extract textures, both from the background of the images and of the TB colonies. The deeper convolutional layers, in turn, detect cord-shaped elements, which are more abstract, high level features.

We have shown that by training the model on two laboratory datasets and using a third laboratory dataset as a validation set, the model generates features that are practically

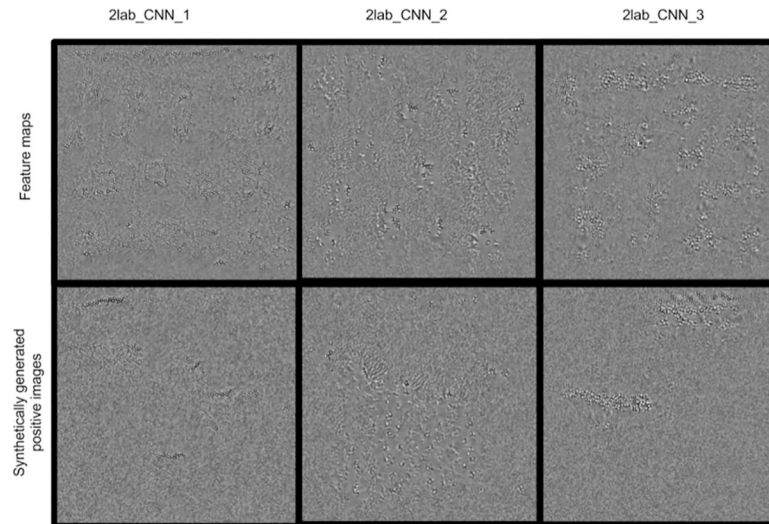


**Fig 5. Features learnt and images synthetically generated by the 2lab\_CNN model.** Top: features extracted from model trained on the three different datasets; bottom: synthetically generated positive images, as mentioned above.

<https://doi.org/10.1371/journal.pone.0212094.g005>

indistinguishable from one laboratory pair to another. This suggests that the model optimises features that are general across laboratories, and supports our hypothesis that our model can generalise and scale on larger datasets and different settings.

Finally, not only do the features from models trained on different laboratory datasets resemble each other: by generating synthetic positive and negative images, we have shown that these features can also be identified in the synthetically generated positive images, which supports the hypothesis that the features are essential to the model's classification. Within the generated images, cord-like elements are identifiable. They appear spaced out, and seem to be surrounded by a lighter region. This brightness variation creates contrasts between the background and the features themselves. After closer inspection of the positive training images, this illumination change is visible but less evident than in the synthetically generated images, which would appear to indicate that the CNN considers it as an important parameter for adequate classification. It is also interesting to note that our previous study had identified this parameter (illumination characteristics) as well as the geometric cording characteristics as being the main predictors of images belonging to the positive class, in our logistic regression model [8]. These features are especially visible when extracted from the model trained on the whole dataset (resc\_CNN). This would indicate that the model's performance is closely related to the optimization of the extracted features, as is the case with human expert diagnosticians.

With regards to our models trained on held-out datasets, even in comparatively small datasets (for e.g., paired-dataset 2), where the number of training samples represents only half of the number of validation samples, the model achieved about 91% and 94% sensitivity and specificity, respectively. This, as well as the low standard deviations across the five testing sets, suggests that our CNN's features have converged.

It is also noteworthy that the 2lab\_CNN model that performed best (2lab\_CNN\_1) had been trained on 8092 low quality images from Callao and Trujillo, and validated on high quality images from UPCH. The two other models performed somewhat worse, despite having been partly trained on high quality images from UPCH, where the training set was of 3400 and 5518 images for models 2 and 3, respectively. Altogether, this data suggests that although the data quality affects the model's ability to learn features, the amount of training data available is an important limiting factor for model optimization. Hence, to perform a fair and definitive

assessment of the model's robustness, a larger and more balanced dataset of images will be required.

Prior to the use of CNNs, there have been efforts devoted to the development of machine-learning tools to facilitate TB diagnostics [33–36]. These were intended to palliate the lack of radiology and microbiological interpretation expertise in many underserved areas of the world. These tools have often been used to detect pulmonary TB from chest radiographies [33–36], and less frequently, directly from sputum samples.

Diagnostics based on chest radiographies rely on posterior anterior chest radiographies, which various machine-learning tools can examine for patterns suggestive of TB [34,35]. Additional information, such as symptoms, can also be included as part of the algorithm's inputs [34]. For the sake of brevity, we note a few examples; readers are directed to by Jaeger et al. [35] for a broader survey of alternative approaches to chest radiography examinations.

Melendez et al. [34] use random forests and extremely randomized trees methods, in combination with clinical information, and achieve 95% sensitivity and 49% specificity. However, these metrics deteriorate when the methods are used separately [34]. Additionally, the combined data-driven approach may influence the diagnostic having clinical information outweigh the image-based interpretation, which could be a result of the training dataset [34]. Xu et al. [36] developed a TB cavity detection system, based on a support vector machine (SVM) for coarse feature classification, a Gaussian model-based template matching, amongst other tools. Despite the extensive image enhancement for feature extraction, the peak sensitivity and specificity are 78.8% and 86.8%, respectively [36]. Other authors have also reported the use SVMs for automated detection of TB, with some success [37].

Melendez et al. [38] recently presented a method of computer-aided detection (CAD) that assists in triage of individuals with suspected active pulmonary TB. When evaluated, it yielded 55.71% specificity at 95% sensitivity, but on dataset comprising of only 87 positive cases, of which 61 were confirmed. Although it is a promising alternative for triage in low TB burden settings, its use in low resource settings is questionable, where access to X-ray equipment might be challenging, and microbiological assays may be more accessible.

Another study by Cao et al. [39] uses an adaptation of the GoogleNet CNN model, pre-trained on the ImageNet dataset and fine tuned on 4701 chest X-Ray images, to achieve 89,6% binary accuracy. It is conceivable that their fine-tuning dataset was insufficient to achieve higher accuracy. There is also no reporting of other relevant metrics. Another study by Cao et al. [40], also using both AlexNet and GoogleNet, finds similar binary accuracy. Here, the Precision, Recall, and F1 score are calculated, and vary quite considerably between validation folds. Additionally, the model is trained on less than 5000 images, and without data augmentation. It is conceivable that, due to large model size, it is simply overfitting. Validation on a held-out dataset, as we performed on our 2lab\_CNN models, is necessary.

Lakhani et al. [33] also use CNNs to analyze chest radiographs, and as did Cao et al., use AlexNet and GoogleNet. Both models demonstrate noteworthy metrics—GoogleNet achieves 92% sensitivity and 98.7% specificity, while AlexNet achieves 92% sensitivity and 94.7% specificity. The performance is similar when both models' decisions are taken into account, but the performance is notably boosted when the diagnostic is Radiologist-augmented. Although the metrics are impressive, here too the model was trained on limited data—1007 total patients, 150 used for testing (75/75 positive/negative). Additionally, there was a lack of validation on a held-out laboratory dataset, although the authors did have 4 independent datasets to work with, which would have provided interesting insight as to their models' ability to generalize.

Lopes et al. [41] provide an interesting attempt to benchmark the performance of some famous CNN architectures on 4 TB datasets, individually and as methods of feature extraction for posterior TB diagnostics by a SVM. The data used was from public datasets of X-ray

images. The best accuracies were obtained from models that combined feature extraction by the CNN (GoogleNet / ResNet / VggNet) and classification by SVM, and range from 76,2% to 84,7%. These metrics are also inferior to ours, and this might be explained by the reduced size of available datasets used for benchmarking.

Hwang et al. [42] base their CNN model on AlexNet, and similarly to the previous studies, use transfer learning for model initialization. They use 3 datasets to evaluate their model, and achieve 90% accuracy across these datasets. Interestingly, they perform a “cross-dataset” experiment, which is analogous to our experiments with models trained on held out datasets. However, their accuracies fall to 83%, while we have shown almost identical metrics between our general model to our held-out dataset models. This study is interesting, and differs from the previous ones, in that it uses a relatively large dataset (more than 10'000 images), which might explain the model's laudable performance.

Jaeger et al. [35] note a few issues with diagnostic tools based on the analysis of radiography images: there is a lack of a common dataset, which in turn causes the inability to compare classifiers; these approaches are inherently indirect diagnostic methods, and may require confirmation through biochemical or visual methods; they often may require extensive preprocessing (for instance, bone suppression, or lung boundary detection); and lastly, the characteristics used for image analysis are often present in other diseases [35]. We would also suggest that it is debatable whether a chest radiography approach would truly be more available in low resource settings, or remote communities.

A less common approach is the direct identification of TB in growth medium, often through recognition of its distinctive growth characteristics. In fact, we were unable to find peer-reviewed, published references that made use of this alternative. We have argued, as was detailed in the previous sections, that our approach harnesses the inherent strengths of CNNs, while also avoiding the pitfalls of extensive image processing, feature selection, and other confounding factors.

In addition to the aforementioned advantages that CNNs have over other machine-learning methods, it has been suggested that deep networks are robust to label noise [43–45]. Some models perform better on non-curated datasets [46]. There is also evidence that CNNs are robust to label noise that is spread randomly across training sets [47]. However, this is controversial, and still to be studied extensively. It is important to highlight that, although different approaches are available for TB diagnostics, these have not been developed specifically for MODS culture image analysis, which is the main interest of this study, given the importance of MODS as explained above.

Amongst the methods that utilize microbiological image analysis, is our previous attempt at an algorithm for MODS interpretation, based on a logistic model classification of extracted features. This algorithm achieved 99.1% sensitivity and 99.7% specificity [8]. However, these metrics were estimated on images of the UPCH laboratory and after extensive image processing. This high quality dataset of images is not fully representative of the images obtainable during field-validation. We observed that the morphological / illumination characteristics of the background on the MODS digital images varied considerably within the 3 mentioned laboratories. This is probably due to the variability in the microbiological processing of the samples. Due to the aforementioned reasons, this approach is limited to functioning site-specifically. Therefore, this algorithm needs to be re-trained each time it is to be used at a different laboratory, with data provided in advance.

To avoid these issues, we trained our CNN on images provided by 3 different laboratories. This allows for features to be selected according to their capacity to help identify MTB growth, regardless of its site of origin. This is possible because of the intrinsic property of CNN convolutional layers to generate and optimise learnable high-level features [10–12], fine-tuned according to their capacity to perform the required classification at scale.

The aforementioned approaches are encouraging and represent significant advances in providing access to affordable, timely TB diagnostics, but have inherent limitations, which our method lacks. Briefly, diagnostics tools based on radiography images are frequently dependent on TB confirmation through other methods, often require extensive image preprocessing, and it is also improbable that the equipment to perform X-Ray radiographies are available in low resource settings. Alternative microbiological sample-based diagnostics have also been devised, but their application is limited by algorithms that necessitate laboratory-based model re-training. Hence, we consider our approach to be more suitable in low resource settings, as facilitates the coordination of an accessible and rapid TB culture strategy, in MODS, with a high performance telediagnosics method, in our CNN. We have already shown that this coordination performs well, with the implementation of a Web-based platform—the particular feature allowing for logistic regression-based TB diagnostics is available here: <http://www.upch.edu.pe/bioinformatic/portal/tuberculosis/>.

We believe that, as we collect more data and train the general model, its robustness will become sufficient to overcome the need for laboratory-specific retraining.

We anticipate that this tool will be key in facilitating access to quick and reliable diagnostic of tuberculosis, and are currently exploring directions in which further work is needed. For instance, the further optimization of the architecture; the training of the reference model on larger and more balanced datasets of MODS digital images; and the possible implementation of a real-time, video monitoring system of MODS samples for possible growth of MTB.

## Conclusions

We have demonstrated the effectiveness of our system for automatic diagnosis of TB, using a CNN trained on 12510 images of 7–10 days MODS cultured samples, both with and without the growth presence of MTB. The images were obtained from three different laboratories, and despite their considerable variability, the CNN achieved 96.63 +/- 0.35% accuracy, 94.74 +/- 0.89% sensitivity and 97.83 +/- 1.07% specificity. Importantly, it performed robustly when validated across held-out laboratory datasets, and showing metrics comparable to those of the model trained on the whole dataset. We anticipate that the model will be improved upon with data from new laboratories. The model's learned features resemble visual cues used by expert diagnosticians to interpret MODS cultures, suggesting that our model may have the ability to generalize and scale. We hope that the system will facilitate access to a reliable, timely diagnostic of TB, especially needed in low-resource settings.

## Acknowledgments

We would like to thank S. Biswas and C. Beltrán for their helpful discussions and valuable advice. We would like to acknowledge Josué Ortega for his initial support in guiding us through the use of CNN in MODS interpretation.

## Author Contributions

**Conceptualization:** Mirko Zimic.

**Data curation:** Patricia Sheen, Mirko Zimic.

**Formal analysis:** Santiago Lopez-Garnier.

**Funding acquisition:** Patricia Sheen, Mirko Zimic.

**Methodology:** Santiago Lopez-Garnier, Mirko Zimic.

**Resources:** Patricia Sheen, Mirko Zimic.



**Software:** Santiago Lopez-Garnier.

**Supervision:** Mirko Zimic.

**Validation:** Santiago Lopez-Garnier.

**Writing – original draft:** Santiago Lopez-Garnier.

**Writing – review & editing:** Patricia Sheen, Mirko Zimic.

## References

1. World Health Organization. Global Tuberculosis Report 2016 [Internet]. Cdc 2016. 2016. ISBN 978 92 4 156539 4
2. World Health Organization. Global tuberculosis report 2012. Who. 2012; 258. 978 92 4 156450 2
3. Comstock GW. Epidemiology of tuberculosis. *Am Rev Respir Dis.* 1982; 125: 8–15. <https://doi.org/10.1164/arrd.1982.125.3P2.8> PMID: 7073104
4. Van Der Werf MJ, Langendam MW, Huitric E, Manissero D. Multidrug resistance after inappropriate tuberculosis treatment: A meta-analysis. *Eur Respir J.* 2012; 39: 1511–1519. <https://doi.org/10.1183/09031936.00125711> PMID: 22005918
5. World Health Organization. Noncommercial culture and drug susceptibility testing methods for screening patients at risk for multi-drug resistant tuberculosis. 2011;
6. Zhang M, Li SY, Rosenthal IM, Almeida D V., Ahmad Z, Converse PJ, et al. Treatment of tuberculosis with rifamycin-containing regimens in immune-deficient mice. *Am J Respir Crit Care Med.* 2011; 183: 1254–1261. <https://doi.org/10.1164/rccm.201012-1949OC> PMID: 21330452
7. Caviedes L, Lee T, Gilman RH, Sheen P, Spellman E, Lee EH, et al. Rapid, efficient detection and drug susceptibility testing of Mycobacterium tuberculosis in sputum by microscopic observation of broth cultures. *J Clin Microbiol.* 2000; 38: 1203–1208. Available: <http://jcm.asm.org/content/38/3/1203.abstract> PMID: 10699023
8. Alva A, Aquino F, Gilman RH, Olivares C, Requena D, Gutiérrez AH, et al. Morphological characterization of Mycobacterium tuberculosis in a MODS culture for an automatic diagnostics through pattern recognition. *PLoS One. Public Library of Science;* 2013; 8: 1–11. <https://doi.org/10.1371/journal.pone.0082809> PMID: 24358227
9. Szegedy C, Liu W, Jia Y, Sermanet P. Going deeper with convolutions. *arXiv Prepr arXiv 14094842.* 2014; 1–9. <https://doi.org/10.1109/CVPR.2015.7298594>
10. LeCun Y, Bengio Y, Hinton G. Deep learning. *Nature.* 2015; 521: 436–444. <https://doi.org/10.1038/nature14539> PMID: 26017442
11. Krizhevsky A, Sutskever I, Hinton GE. ImageNet Classification with Deep Convolutional Neural Networks. *Adv Neural Inf Process Syst.* 2012; 1–9. <http://dx.doi.org/10.1016/j.protcy.2014.09.007>
12. Lee H, Grosse R, Ranganath R, Ng AY. Convolutional deep belief networks for scalable unsupervised learning of hierarchical representations. *Proc 26th Annu Int Conf Mach Learn ICML 09.* 2009; 2008: 1–8. <https://doi.org/10.1145/1553374.1553453>
13. Ciresan D, Meier U. Multi-column Deep Neural Networks for Image Classification. *IEEE Conf Comput Vis Pattern Recognit.* 2012; 3642–3649. <https://doi.org/10.1109/CVPR.2012.6248110>
14. He K, Zhang X, Ren S, Sun J. Delving deep into rectifiers: Surpassing human-level performance on imagenet classification. *Proc IEEE Int Conf Comput Vis.* 2016; 11–18–Dece: 1026–1034. <https://doi.org/10.1109/ICCV.2015.123>
15. Pinto N, Doukhan D, DiCarlo JJ, Cox DD. A high-throughput screening approach to discovering good forms of biologically inspired visual representation. *PLoS Comput Biol.* 2009; 5. <https://doi.org/10.1371/journal.pcbi.1000579> PMID: 19956750
16. Mnih V, Kavukcuoglu K, Silver D, Rusu AA, Veness J, Bellemare MG, et al. Human-level control through deep reinforcement learning. *Nature.* Nature Publishing Group, a division of Macmillan Publishers Limited. All Rights Reserved.; 2015; 518: 529–533. Available: <http://dx.doi.org/10.1038/nature14236> PMID: 25719670
17. Silver D, Huang A, Maddison CJ, Guez A, Sifre L, van den Driessche G, et al. Mastering the game of Go with deep neural networks and tree search. *Nature.* Nature Publishing Group, a division of Macmillan Publishers Limited. All Rights Reserved.; 2016; 529: 484–489. Available: <http://dx.doi.org/10.1038/nature16961> PMID: 26819042

18. Esteva A, Kuprel B, Novoa RA, Ko J, Swetter SM, Blau HM, et al. Dermatologist-level classification of skin cancer with deep neural networks. *Nature*. Nature Publishing Group; 2017; 1–11. <https://doi.org/10.1038/nature21056>
19. Zhang W, Li R, Deng H, Wang L, Lin W, Ji S, et al. Deep convolutional neural networks for multi-modal intensity infant brain image segmentation. *Neuroimage*. 2015; 108: 214–224. <http://dx.doi.org/10.1016/j.neuroimage.2014.12.061> PMID: 25562829
20. Razavian N, Sontag D. Temporal Convolutional Neural Networks for Diagnosis from Lab Tests. *CoRR*. 2015;abs/1511.0. Available: <http://arxiv.org/abs/1511.07938>
21. Xiangyu Chen, Yanwu Xu, Damon Wing Kee Wong, Tien Yin Wong, Jiang Liu. Glaucoma detection based on deep convolutional neural network. 2015 37th Annual International Conference of the IEEE Engineering in Medicine and Biology Society (EMBC). IEEE; 2015. pp. 715–718. <https://doi.org/10.1109/EMBC.2015.7318462>
22. Abdel-Zaher AM, Eldeib AM. Breast cancer classification using deep belief networks. *Expert Syst Appl*. Pergamon Press, Inc.; 2016; 46: 139–144. <https://doi.org/10.1016/j.eswa.2015.10.015>
23. Xie W, Li Y, Ma Y. Breast mass classification in digital mammography based on extreme learning machine. *Neurocomputing*. Elsevier; 2016; 173: 930–941. <https://doi.org/10.1016/j.neucom.2015.08.048>
24. Chollet F. Keras. GitHub; 2015.
25. Theano Development Team. Theano: A {Python} framework for fast computation of mathematical expressions. *arXiv e-prints*. 2016;abs/1605.0. Available: <http://arxiv.org/abs/1605.02688>
26. Simonyan K, Zisserman A. Very Deep Convolutional Networks for Large-Scale Image Recognition. *Int Conf Learn Represent*. 2015; 1–14. <https://doi.org/10.1016/j.infsof.2008.09.005>
27. Jarrett K, Kavukcuoglu K, Ranzato M, LeCun Y. What is the best multi-stage architecture for object recognition? *Proc IEEE Int Conf Comput Vis*. 2009; 2146–2153. <https://doi.org/10.1109/ICCV.2009.5459469>
28. Zeiler MD, Fergus R. Visualizing and understanding convolutional networks. *Lect Notes Comput Sci (including Subser Lect Notes Artif Intell Lect Notes Bioinformatics)*. 2014;8689 LNCS: 818–833. [https://doi.org/10.1007/978-3-319-10590-1\\_53](https://doi.org/10.1007/978-3-319-10590-1_53)
29. Ioffe S, Szegedy C. Batch Normalization: Accelerating Deep Network Training by Reducing Internal Covariate Shift. *CoRR*. 2015;abs/1502.0. Available: <http://arxiv.org/abs/1502.03167>
30. Hinton GE, Srivastava N, Krizhevsky A, Sutskever I, Salakhutdinov RR. Improving neural networks by preventing co-adaptation of feature detectors. *ArXiv e-prints*. 2012; 1–18. arXiv:1207.0580
31. Chollet F. How convolutional neural networks see the world. In: *The Keras Blog [Internet]*. 2016 [cited 9 Nov 2017]. Available: <https://blog.keras.io/how-convolutional-neural-networks-see-the-world.html>
32. Yosinski J, Clune J, Nguyen A, Fuchs T, Lipson H. Understanding Neural Networks Through Deep Visualization. *Int Conf Mach Learn—Deep Learn Work* 2015. 2015; 12. Available: <http://arxiv.org/abs/1506.06579>
33. Lakhani P, Sundaram B. Deep Learning at Chest Radiography: Automated Classification of Pulmonary Tuberculosis by Using Convolutional Neural Networks. *Radiology*. 2017; 284: 574–582. <https://doi.org/10.1148/radiol.2017162326> PMID: 28436741
34. Melendez J, Sánchez CI, Philipsen RHHM, Maduskar P, Dawson R, Theron G, et al. An automated tuberculosis screening strategy combining X-ray-based computer-aided detection and clinical information. *Nat Publ Gr*. 2016; <https://doi.org/10.1038/srep25265>
35. Jaeger S, Karargyris A, Candemir S, Siegelman J, Folio L, Antani S, et al. Automatic screening for tuberculosis in chest radiographs: a survey. *Quant Imaging Med Surg*. AME Publications; 2013; 3: 89–99. <https://doi.org/10.3978/j.issn.2223-4292.2013.04.03> PMID: 23630656
36. Xu T, Cheng I, Long R, Mandal M. Novel coarse-to-fine dual scale technique for tuberculosis cavity detection in chest radiographs. *EURASIP J Image Video Process*. Springer International Publishing; 2013; 2013: 3. <https://doi.org/10.1186/1687-5281-2013-3>
37. Jaeger S, Karargyris A, Candemir S, Folio L, Siegelman J, Callaghan F, et al. Automatic Tuberculosis Screening Using Chest Radiographs. *IEEE Trans Med Imaging*. 2014; 33: 233–245. <https://doi.org/10.1109/TMI.2013.2284099> PMID: 24108713
38. Melendez J, Hogeweg L, Sánchez CI, Philipsen RHHM, Aldridge RW, Hayward AC, et al. Accuracy of an automated system for tuberculosis detection on chest radiographs in high-risk screening. *Int J Tuberc Lung Dis*. The International Union Against Tuberculosis and Lung Disease; 2018; 22: 567–571. <https://doi.org/10.5588/ijtld.17.0492> PMID: 29663963
39. Cao Y, Liu C, Liu B, Brunette MJ, Zhang N, Sun T, et al. Improving Tuberculosis Diagnostics Using Deep Learning and Mobile Health Technologies among Resource-Poor and Marginalized Communities.

- 2016 IEEE First International Conference on Connected Health: Applications, Systems and Engineering Technologies (CHASE). IEEE; 2016. pp. 274–281. <https://doi.org/10.1109/CHASE.2016.18>
40. Liu C, Cao Y, Alcantara M, Liu B, Brunette M, Peinado J, et al. TX-CNN: Detecting tuberculosis in chest X-ray images using convolutional neural network. 2017 IEEE International Conference on Image Processing (ICIP). IEEE; 2017. pp. 2314–2318. <https://doi.org/10.1109/ICIP.2017.8296695>
  41. Lopes UK, Valiati JF. Pre-trained convolutional neural networks as feature extractors for tuberculosis detection. *Comput Biol Med.* 2017; 89: 135–143. <https://doi.org/10.1016/j.combiomed.2017.08.001> PMID: 28800442
  42. Hwang S, Kim H-E, Jeong J, Kim H-J. A novel approach for tuberculosis screening based on deep convolutional neural networks. In: Tourassi GD, Armato SG, editors. 2016. p. 97852W. <https://doi.org/10.1117/12.2216198>
  43. Bansal A, Castillo C, Ranjan R, Chellappa R. The Do's and Don'ts for CNN-Based Face Verification. 2017 IEEE Int Conf Comput Vis Work. IEEE; 2017; 2545–2554. <https://doi.org/10.1109/ICCVW.2017.299>
  44. Yuan J, Ma W, Zhu P, Egiazarian K. Robust Deep Face Recognition with Label Noise. Springer, Cham; 2017. pp. 593–602. [https://doi.org/10.1007/978-3-319-70096-0\\_61](https://doi.org/10.1007/978-3-319-70096-0_61)
  45. Rolnick D, Veit A, Belongie S, Shavit N. Deep Learning is Robust to Massive Label Noise. 2017; Available: <https://arxiv.org/abs/1705.10694>
  46. Parkhi OM, Vedaldi A, Zisserman A. Deep Face Recognition. Proceedings of the British Machine Vision Conference 2015. 2015. p. 41.1–41.12. <https://doi.org/10.5244/C.29.41>
  47. Drory A, Avidan S, Giryas R. On the Resistance of Neural Nets to Label Noise. 2018; Available: <https://arxiv.org/pdf/1803.11410.pdf>